

Structural aspects of FRG in quantum tunnelling computations

Alfio Bonanno*

*INAF, Osservatorio Astrofisico di Catania,
via S.Sofia 78, I-9 5123 Catania, Italy;
INFN, Sezione di Catania, via S. Sofia 64, I-95123, Catania, Italy*

Alessandro Codello†

*Instituto de Física, Facultad de Ingeniería,
Universidad de la República, 11000 Montevideo, Uruguay*

Dario Zappalà‡

INFN, Sezione di Catania, Via Santa Sofia 64, 95123 Catania, Italy
(Dated: June 15, 2022)

Abstract

ABSTRACT

We probe both the unidimensional quartic harmonic oscillator and the double well potential through a numerical analysis of the Functional Renormalization Group flow equations truncated at first order in the derivative expansion. The two partial differential equations for the potential $V_k(\varphi)$ and the wave function renormalization $Z_k(\varphi)$, as obtained in different schemes and with distinct regulators, are studied down to $k = 0$, and the energy gap between lowest and first excited state is computed, in order to test the reliability of the approach in a strongly non-perturbative regime. Our findings point out at least three ranges of the quartic coupling λ , one with higher λ where the lowest order approximation is already accurate, the intermediate one where the inclusion of the first correction produces a good agreement with the exact results and, finally, the one with smallest λ where presumably the higher order correction of the flow is needed. Some details of the specifics of the infrared regulator are also discussed.

PACS numbers:

*Electronic address: alfio.bonanno@inaf.it

†Electronic address: acodello@fing.edu.uy

‡Electronic address: dario.zappala@ct.infn.it

I. INTRODUCTION

In spite of the enormous success of functional renormalization group (FRG) approach in statistical mechanics and quantum field theory (see [1] for a recent review), its applicability to strongly non-perturbative problems is not obvious. In particular, the calculation of the energy gap ΔE between the first excited state and the ground state for the anharmonic oscillator is an important test to study the effectiveness of the FRG approach to capture genuine topological effects. This model is based on the one particle Hamiltonian with potential (here φ indicates the coordinate of the particle) :

$$V(\varphi) = \frac{M^2}{2} \varphi^2 + \lambda \varphi^4 \quad (1)$$

which corresponds to the anharmonic oscillator with quartic corrections if $M^2 > 0$, or to the double well potential if $M^2 < 0$. In the following, we express all dimensionful quantities in terms of the square mass scale $|M^2|$, which is equivalent to choose either $M^2 = 1$ or $M^2 = -1$.

In the former case, a quartic term is added to the exactly solvable harmonic oscillator Hamiltonian, and therefore a perturbative treatment of the problem is suitable as long as the quartic coupling does not grow too large. In the latter case, the quadratic part is unstable and the stabilizing quartic term produces a double well that becomes deeper and deeper when $\lambda \rightarrow 0$. This means that the effect of the tunnelling of the wave function becomes more important for $\lambda \rightarrow 0$, and therefore in this limit any perturbative approach fails to produce reasonable results.

A reliable approach to confront the $M^2 = -1, \lambda \rightarrow 0$ problem is the dilute instanton gas calculation [2, 3] that produces the well known, non-analytic exponential expression of the energy gap ΔE between first excited and ground state

$$\Delta E_{inst} = 2 \left(\frac{2\sqrt{2}}{\pi\lambda} \right)^{1/2} e^{-(3\lambda\sqrt{2})^{-1}} \quad (2)$$

Clearly, the quantum mechanical problem, either with $M^2 = 1$ or $M^2 = -1$, can be solved through the numerical determination of the eigenvalues of the associated Schrödinger equation which then provides the exact reference values of ΔE_{exact} at each value of λ .

Consequently, the calculation of ΔE represents an important challenge for the FRG approach, in particular for low values of λ . Moreover, this analysis can be regarded as an essential step toward the application of the FRG to more complex problems regarding the estimate of false vacuum decay rates in quantum field theory[4] and, more specifically, concerning the stability of the electroweak vacuum, related to the Ultraviolet (UV) completion of the Standard Model, and the study of inflationary models in cosmology [5], because in these contexts the typical approach adopted mainly relies on instanton calculation (see e.g. [6, 7]).

Early works started the investigation of this problem by means of a sharp cut-off FRG in the local potential approximation (LPA), either within a polynomial truncation of the resulting flow equation for the potential [8, 9], or by direct numerical resolution of the local potential flow equation [10]. The inclusion of a field dependent wave-function renormalization $Z(\phi)$ first appeared in [11] by means of a Schwinger's proper-time cutoff in the FRG equation. In that work a numerical integration of the combined system of non-linear parabolic Partial Differential Equations (PDE) for the local potential $V(\phi)$ and $Z(\phi)$ was employed.

In fact, polynomial truncations of the FRG generate a system of differential equations which is singular in the $k \rightarrow 0$ limit in the broken phase. On the contrary, the full set of PDE correctly reproduces the discontinuity in the correlation length below the critical temperature [12] but the

numerical integration is not straightforward, as one has to resort to implicit methods for a class of coupled non-linear parabolic evolution equation [13, 14]. In $d = 1$ dimensions the evolution of flow in the infrared is less severe and one can hope that already with the familiar *method of the lines* (MoL) [15], it is possible to reach values of λ small enough to render the comparison with standard dilute instanton gas approach meaningful. In [16], FRG with smooth and sharp cut-off have been solved with both polynomial truncation and MoL but some discrepancies between the findings of [16] and [11] for very small λ have emerged. Further applications of FRG to supersymmetric quantum mechanics have appeared in [17]. An attempt to apply the Principle of Minimal Sensitivity in this context has recently been discussed in [18].

Beyond LPA a number of structural aspects in the formulation of FRG arise. In the case of the so called *spectrally adjusted* (SA) flow the coarse-graining procedure is built in terms of the eigenvalues of the spectrum of $\Gamma_k^{(2)}$ evaluated at the background field [19], where Γ_k is the effective average action at the scale k . The spectrum is therefore not fixed but computed at the running cutoff k . If we visualize the averaging procedure in real space, the use of a running cutoff built with a running blocked field can be thought as the analogous of a "lagrangian" description of the dynamic of the fluid made by a co-moving observer. On the contrary the "eulerian" coarse-grained flow is produced if, in lowering the cutoff from k to $k - \Delta k$, a *fixed* spectrum of the Laplacian operator \square is employed at each k . Clearly both "lagrangian" and "eulerian" schemes lead to very similar results near criticality when the anomalous dimension is small, but it is not clear which scheme is to be expected to work better in general.

From this point of view we would like to stress that, strictly speaking, only FRG with *not spectrally adjusted* (NSA) regulators are "exact" flow in the sense of [20, 21], while SA regulators, albeit widely used in the FRG literature, are not in general exact unless they are derived from a much more involved and non-linear flow equation which we will not consider in this paper [22].

The aim of this work is twofold. First, we would like to address the computation of ΔE in the small λ regime, by means of distinct formulations, namely the Exact Renormalization Group (ERG) flow equations characterized by the theta-function regulator proposed in [23] and the Schwinger's Proper Time (PT) flow equations introduced in [24–26], in order to get an inclusive prediction of ΔE from the FRG. This point is essential both to test the reliability of this approach in the deep non-perturbative regime ($\lambda \ll 1$), especially in comparison with the instanton gas calculation, and, at the same time, to produce a countercheck on the mentioned discrepancy with the analysis of [16]. Second, we intend to study the impact of SA *vs.* NSA cutoff in the low λ region for these type of FRG. In particular, in the case of the PT flow, we further discuss the dependence of the various cutoff schemes introduced in [27].

The structure of the paper is the following. In Sect. II we review the structure of the flow equations that are subsequently integrated and, more specifically, Sect. II A is devoted to the ERG flow, while in Sect. II B the PT equations are discussed. Then, in Sect. III the results of our numerical analysis are presented, first considering the LPA approximation in III B, and by including the wave function renormalization in III C. Our conclusions are reported in Sect. IV.

II. FLOW EQUATIONS

A. ERG flow

We shall first consider the implementation of the ERG flow [1] (we define the RG 'time' as $t = \log(k/\Lambda)$, where k is the running energy scale and Λ is a fixed UV cutoff)

$$\partial_t \Gamma_k[\varphi] = \frac{1}{2} \text{Tr} \left[\partial_t R_k(q^2) G_k(q^2, \varphi) \right] \quad (3)$$

and the regularized propagator $G_k(q^2, \varphi)$ is

$$G_k(q^2, \varphi) = \frac{1}{\Gamma_k^{(2)}(q^2, \varphi) + R_k(q^2)} = \frac{1}{Z_k(\varphi) q^2 + V_k''(\varphi) + R_k(q^2)}. \quad (4)$$

$R_k(q^2)$ is the regulator of the infrared modes which will be specified below. $\Gamma_k^{(2)}(q^2, \varphi)$ indicates the second functional derivative of $\Gamma_k[\varphi]$ with respect to the field φ . Here and below, prime, double prime, etc. indicate one, two, etc. derivatives with respect to the argument.

The explicit form adopted for the running effective action $\Gamma_k[\varphi]$ comes from the first non trivial order of its derivative expansion:

$$\Gamma_k[\varphi] = \int d^d x \left[V_k(\varphi) + \frac{1}{2} Z_k(\varphi) (\partial\varphi)^2 \right] + O(\partial^4) \quad (5)$$

and we focus on the flows of V_k and Z_k , which are derived from the flow of the two-point function

$$\begin{aligned} \partial_t \Gamma_k^{(2)}(p^2) &= \partial_t Z_k p^2 + \partial_t V_k'' = \\ \int_q \left[\Gamma_k^{(3)}(q, p, -q-p) \right]^2 G_k((q+p)^2) G_k^2(q^2) \partial_t R_k(q^2) &- \frac{1}{2} \int_q \Gamma_k^{(4)}(q, p, -p, -q) G_k^2(q^2) \partial_t R_k(q^2) = \\ \int_q \left[Z_k'(q^2 + q \cdot p + p^2) + V_k'''' \right]^2 G_k((q+p)^2) G_k^2(q^2) \partial_t R_k(q^2) & \\ - \frac{1}{2} \int_q \left[Z_k''(q^2 + p^2) + V_k'''' \right] G_k^2(q^2) \partial_t R_k(q^2) & \end{aligned} \quad (6)$$

by respectively extracting the $O(p^0)$ and $O(p^2)$ coefficients in the expansion of the left hand side (lhs) of Eq. (6) in powers of momentum p . Incidentally, we notice that in Eq. (6) the symmetry $\Gamma_k^{(3)}(q, p, -q-p) = \Gamma_k^{(3)}(q+p, -p, -q)$ is used to simplify the first contribution (diagram).

Therefore, we need to expand the propagator $G_k((q+p)^2)$ in Eq. (6), in powers of p

$$G_k((q+p)^2) = G_k(q^2) + 2xq G_k'(q^2)p + [G_k'(q^2) + 2x^2 q^2 G_k''(q^2)] p^2 + O(p^3). \quad (7)$$

where we recall that primes indicate derivative with respect to the argument and we labelled the cosine of the angle between the four-vectors p and q , as x .

Then, by definition, the derivatives of the regularized propagator are

$$G_k' = -G_k^2 (Z_k + R_k') \quad G_k'' = 2G_k^3 (Z_k + R_k')^2 - G_k^2 R_k'' \quad (8)$$

and we can insert Eqs. (7), (8) into Eq. (6), to obtain the flow equations for V_k and Z_k

$$\partial_t V_k = \mathcal{B}_V^d(V_k'', Z_k) \quad \partial_t Z_k = \mathcal{B}_Z^d(V_k'', V_k''', Z_k, Z_k', Z_k'') \quad (9)$$

where the explicit expressions for the right hand side (rhs) are

$$(4\pi)^{\frac{d}{2}} \mathcal{B}_V^d = \frac{1}{2} Q_{\frac{d}{2}} [G_k \partial_t R_k] \quad (10)$$

and

$$\begin{aligned} (4\pi)^{\frac{d}{2}} \mathcal{B}_Z^d &= (V_k''')^2 \left\{ Q_{\frac{d}{2}} [G_k^2 G_k' \partial_t R_k] + Q_{\frac{d}{2}+1} [G_k^2 G_k'' \partial_t R_k] \right\} \\ &+ Z_k' V_k'''' \left\{ 2Q_{\frac{d}{2}} [G_k^3 \partial_t R_k] + (d+2)Q_{\frac{d}{2}+1} [G_k^2 G_k' \partial_t R_k] \right. \\ &\quad \left. + (d+2)Q_{\frac{d}{2}+2} [G_k^2 G_k'' \partial_t R_k] \right\} \\ &+ (Z_k')^2 \left\{ \frac{2d+1}{2} Q_{\frac{d}{2}+1} [G_k^3 \partial_t R_k] + \frac{(d+2)(d+4)}{4} Q_{\frac{d}{2}+2} [G_k^2 G_k' \partial_t R_k] \right. \\ &\quad \left. + \frac{(d+2)(d+4)}{4} Q_{\frac{d}{2}+3} [G_k^2 G_k'' \partial_t R_k] \right\} \\ &+ Z_k'' \left\{ -\frac{1}{2} Q_{\frac{d}{2}} [G_k^2 \partial_t R_k] \right\} \end{aligned} \quad (11)$$

and the Q -functionals of variable $z = q^2$ are defined as:

$$Q_n[f] \equiv \frac{1}{\Gamma[n]} \int_0^\infty dz z^{n-1} f(z) \quad (12)$$

So far, all relations are valid for an arbitrary cutoff function and in any dimension. Now, we specify the function $R_k(z)$ by taking Litim's regulator [23], in two different forms, namely in the plain NSA version

$$R_k^{NSA}(z) = (k^2 - z) \theta(k^2 - z) \quad (13)$$

and in the SA form that includes a field dependent wave-function renormalization prefactor

$$R_k^{SA}(z) = Z_k(\varphi) (k^2 - z) \theta(k^2 - z), \quad (14)$$

and $\theta(x)$ is the Heaviside function.

In the NSA case, only a partial cancellation of the square momentum z dependence of $G_k(z)$ is realized, with the residual dependence weighted by the deviation of the factor $Z_k(\varphi)$ from 1 :

$$G_k(z) = \frac{1}{Z_k z + (k^2 - z) \theta(k^2 - z) + V_k''} \quad (15)$$

and the replacement of Eqs. (13), (15) into Eqs. (12), (10) and (11) leads us to a coupled pair of flow equations for V_k and Z_k , where the integration over the variable z in Eq. (12) produces a long and involved sum of Hypergeometric functions, due to the not full momentum simplification in Eq. (15). Still, in this case, it is possible to recover an explicit, analytic form, suitable for numerical integration (which is discussed in the next Section), of the partial differential equations (PDE) governing the flow of V_k and Z_k , that, for the sake of simplicity, we do not display here.

The SA regulator displayed in (14) instead produces a much simpler structure of the flow equations, thanks to the presence of $Z_k(\varphi)$ in $R_k^{SA}(z)$. In fact, in this case the propagator reduces to the square momentum z independent quantity $H_k^{-1}(\varphi)$:

$$G_k(z) = \frac{1}{Z_k z + Z_k (k^2 - z) \theta(k^2 - z) + V_k''} \rightarrow \frac{1}{Z_k k^2 + V_k''} \equiv \frac{1}{H_k} \quad (16)$$

and the corresponding Q -functionals entering \mathcal{B}_V^d and \mathcal{B}_Z^d , have the following simple form:

$$Q_n[G_k^m \partial_t R_k] = \frac{k^{2(n-m+1)}}{\Gamma(n)} \frac{Z_k}{(Z_k + \omega_k)^m} \left\{ \frac{2 - \eta_k}{n} + \frac{\eta_k}{n+1} \right\} \quad (17)$$

$$Q_n[G_k^m G_k' \partial_t R_k] = 0 \quad (18)$$

$$Q_n[G_k^m G_k'' \partial_t R_k] = -\frac{k^{2(n-m-2)}}{\Gamma(n)} \frac{Z_k^2}{(Z_k + \omega_k)^{m+2}} \quad (19)$$

where we used the specific value of Heaviside function at the origin, $\theta(0) = 1/2$, and we defined $\omega_k \equiv V_k''/k^2$ and the field and scale dependent $\eta_k(\varphi)$ (recall $t = \log(k/\Lambda)$) as

$$\eta_k(\varphi) \equiv -\partial_t \log Z_k(\varphi), \quad (20)$$

that must not be mistaken for the field anomalous dimension at criticality. Then for the SA case, Eqs. (14), (17), (18), (19), and (16) yield the following \mathcal{B} -functions in $d = 1$, to be inserted in Eq. (10)

$$\mathcal{B}_V^{d=1} = \frac{Z_k k^3}{\pi H_k} (1 - \eta_k/3) \quad (21)$$

$$\mathcal{B}_Z^{d=1} = \frac{Z_k k^3}{\pi H_k} \cdot \left\{ \left(-\frac{Z_k''}{H_k} + \frac{4Z_k' V_k'''}{H_k^2} \right) \left(1 - \frac{\eta_k}{3} \right) + \frac{2(Z_k')^2 k^2}{H_k^2} \left(1 - \frac{\eta_k}{5} \right) - \frac{Z_k (V_k''')^2}{H_k^3} - \frac{2k^2 Z_k Z_k' V_k'''}{H_k^3} - \frac{Z_k (Z_k')^2 k^4}{H_k^3} \right\} \quad (22)$$

Despite the compact form of the flow equations displayed in Eqs. (21) and (22), we notice that terms proportional to η_k introduce nonlinear effects related to the 'time' derivative of Z_k , which are harmless as long as $Z_k \simeq 1$, but become very difficult to handle in the numerical integration when Z_k becomes substantially different from 1, which occurs in the region of very small coupling λ in Eq. (1). Due to this complication, together with the full flow of V_k and Z_k in Eqs. (21) and (22), we shall analyze its reduced version obtained by simply setting $\eta_k = 0$, thus making the flow equations linear both in $\partial_t V_k$ and $\partial_t Z_k$, and therefore much easier to integrate numerically.

B. Proper Time flow

Now, we turn to a different kind of flow, namely the Proper Time (PT) flow, whose equations for V_k and Z_k can be cast in the form of PDE, suitable for numerical investigation. This kind of flow is to be regarded as a particular case of background field flow [28], although recently it was reconsidered as a type of Wilsonian action flow [26, 27], and the corresponding flow equations of V_k and Z_k are discussed in detail in [27]. Here, we do not focus on the nature of the PT flow, as we are rather interested in its application to the spectrum of the double well potential and we refer to [27] for a detailed discussion on the structure of the regulator and on the consequent derivation of the flow equations, both in the NSA and in the SA case.

Here, we just mention that the NSA regulator, which carries no dependence on the renormalization factor Z_k , produces the following flow equation (named "A-scheme" in [27])

$$\partial_t \Gamma_k[\varphi] = -\text{Tr} \left(\frac{m k^2}{\Gamma_k^{(2)}[\varphi] + m k^2} \right)^m. \quad (23)$$

where $m > d/2$ is a free parameter that roughly specifies the sharpness of the regulator, and it is usually taken as integer. Eq. (23) in $d = 1$ and with the same formal parameterization of the action adopted in Eq. (5), reduces to the following NSA coupled flow

$$\partial_t V_k = -\frac{\Gamma(m-1/2)}{2\sqrt{\pi}\Gamma(m)} \sqrt{\frac{m k^2}{Z_k}} \left(\frac{m k^2}{h_{k,m}^{NSA}} \right)^{m-1/2} \quad (24)$$

$$\partial_t Z_k = \frac{\Gamma(m+1/2)}{2\sqrt{\pi}\Gamma(m)} \sqrt{\frac{m k^2}{Z_k}} \left(\frac{m k^2}{h_{k,m}^{NSA}} \right)^{m-1/2} \cdot \left[\frac{Z_k''}{h_{k,m}^{NSA}} + \frac{Z_k (V_k''')^2 (m+1/2)(m+3/2)}{6 (h_{k,m}^{NSA})^3} - \frac{3 Z_k' V_k''' (m+1/2)}{2 (h_{k,m}^{NSA})^2} - \frac{21}{24} \frac{(Z_k')^2}{Z_k h_{k,m}^{NSA}} \right] \quad (25)$$

where $\Gamma(x)$ is the Gamma-function and $h_{k,m}^{NSA}$ is

$$h_{k,m}^{NSA} = m k^2 + V_k'' \quad (26)$$

On the other hand, the SA flow requires the replacement of the scale k^2 with the corrected scale $Z_k(\varphi) k^2$ in the regulator and this produces flow equations indicated in [27] as the 'B-scheme', or as the 'simplified type-C scheme' if the derivatives of the factors $Z_k(\varphi)$ that appear in the regulator are neglected. We refer to [27] for the explicit involved form of the flow equations of V_k and Z_k in the 'B-scheme', while the 'simplified type-C scheme' equations are simply obtained from Eqs. (24) and (25) by replacing everywhere $m k^2 \rightarrow Z_k(\varphi) m k^2$, i.e. we find

$$\partial_t V_k = -\frac{\Gamma(m-1/2)}{2\sqrt{\pi}\Gamma(m)} \sqrt{m k^2} \left(\frac{Z_k m k^2}{h_{k,m}^{SA}} \right)^{m-1/2} \quad (27)$$

$$\partial_t Z_k = \frac{\Gamma(m+1/2)}{2\sqrt{\pi}\Gamma(m)} \sqrt{m k^2} \left(\frac{Z_k m k^2}{h_{k,m}^{SA}} \right)^{m-1/2} \cdot \left[\frac{Z_k''}{h_{k,m}^{SA}} + \frac{Z_k (V_k''')^2 (m+1/2)(m+3/2)}{6 (h_{k,m}^{SA})^3} - \frac{3 Z_k' V_k''' (m+1/2)}{2 (h_{k,m}^{SA})^2} - \frac{21}{24} \frac{(Z_k')^2}{Z_k h_{k,m}^{SA}} \right] \quad (28)$$

with the definition

$$h_{k,m}^{SA} \equiv Z_k m k^2 + V_k'' . \quad (29)$$

We notice that the 'simplified type-C scheme' flow equations (27) and (28) are equal to the pair of equations analyzed in [11] (and previously introduced in [24]), provided that the scale \hat{k} and the parameter \hat{m} , used in [11], are replaced with our k and m , according to $\hat{m} + 1 = m$ and $\hat{k} = k m / \hat{m}$. Clearly, observables calculated in the limit $k \rightarrow 0$ are insensible to the difference between k and \hat{k} , and one can compare the results derived from the two flows for equivalent values of m and \hat{m} .

Computations in [11] were performed with a particular exponential form of the flow obtained in the limit $\hat{m} \rightarrow \infty$. In fact, the same exponential flow equations are recovered from Eqs. (27) and (28) in the limit $m \rightarrow \infty$; however we shall not repeat here the computation of ΔE in this case, but rather look at the PT flow at the reasonably large value $m = 10$, to produce predictions close to those of the exponential flow.

In addition, we notice that the SA version of the PT flow in Eqs. (27) and (28) at the particular value $m = 3/2$, resembles the ERG displayed in Eqs. (21) and (22), at $\eta_k = 0$. Actually, for $m = 3/2$, the flow equations for V_k (27) and (21) coincide, while in the equations for Z_k , only some terms are identical. From the numerical analysis, it will be evident that the differences between the two are subleading and the ERG computation of ΔE falls between the values of ΔE determined with the PT flow at $m = 1$ and $m = 2$.

To summarize, in the next Section we integrate both NSA and SA version of the PT flow, respectively in Eqs. (24) and (25) and in Eqs. (27) and (28) at small values of m , namely at $m = 1, 2, 3, 4$, at which the convergence of the differential equations is more accurate, and also at $m = 10$ which, as already noticed, should produce results that are close to those obtained with the exponential PT flow [11].

III. NUMERICAL RESULTS

A. Preliminary details

As discussed previously, the most accurate determination of the energy gap ΔE comes from the resolution of the eigenvalue problem for the associated Schroedinger equation. In the following, we indicate with ΔE_{exact} the gap computed in this way and display in Table I some determinations both for $M^2 = 1$ and $M^2 = -1$. In the former case, only the two values $\lambda = 1$ and $\lambda = 0.02$ are selected to test the predictions of the RG flow either in a strongly or in a weakly coupled regime. Conversely in the case $M^2 = -1$, where the non-perturbative effect of the tunnelling becomes important, we select more values of the quartic coupling in the range $\lambda = 0.4$ to $\lambda = 0.01$, to have a clear understanding of the RG flow predictions in different regimes.

In Table I, for the double well potential case $M^2 = -1$ we include the data of the gap as obtained from the instanton calculation reported in Eq. (2). It is immediately evident that for $\lambda = 0.04$ or larger, ΔE_{inst} are very far from ΔE_{exact} , and even at $\lambda = 0.03$ we find an error of about 30%. Conversely, the data reported at $\lambda = 0.02, 0.01$ show respectively an error of 10% and 5%. Only for lower values of λ the instanton calculation becomes really precise.

Now, we are interested in obtaining a further determination of ΔE from the numerical resolution of the flow equations for V_k and Z_k down to $k = 0$. In fact, $(\Delta E)^2$ is related to the renormalized curvature of the effective potential at the origin $(V_{k=0}(\varphi)'' / Z_{k=0}(\varphi))|_{\varphi=0}$. However, the resolution of the flow equations when the initial condition (set at a large UV scale $k = \Lambda$) is given by the potential in (1) with $M^2 = -1$ (which is concave downward around $\phi = 0$), usually presents a stiff behavior related to the appearance of a spinodal line. This line is defined by the vanishing of the inverse propagator entering the flow equations: i.e. in our case it is defined by the vanishing of $G_k(z)^{-1}$ in Eq. (15) or of H_k, h_k^{NSA}, h_k^{SA} , respectively defined in Eqs. (16), (26), (29).

$M^2 = 1$			
λ	ΔE_{exact}	–	ΔE_{WH}
1	1.9341	–	1.928(2)
0.02	1.0540	–	1.053(2)
$M^2 = -1$			
λ	ΔE_{exact}	ΔE_{inst}	ΔE_{WH}
0.4	0.9667	1.6645	0.965(2)
0.3	0.8166	1.5792	0.817(2)
0.2	0.6159	1.3058	0.621(2)
0.1	0.2969	0.5683	0.329(2)
0.05	0.0562	0.0761	0.157(2)
0.04	0.0210	0.0262	0.125(2)
0.03	0.0036	0.0042	0.094(1)
0.02	$0.93 \cdot 10^{-4}$	$1.02 \cdot 10^{-4}$	0.063(1)
0.01	$1.05 \cdot 10^{-9}$	$1.10 \cdot 10^{-9}$	0.032(1)

TABLE I: ΔE for various couplings λ and for $M^2 = 1$ or $M^2 = -1$, as obtained from the Schrodinger equation (ΔE_{exact}), the instanton calculation (ΔE_{inst}), and from the Wegner-Houghton flow equation (ΔE_{WH}).

This problem is well known since long time. A systematic way of circumventing was proposed in [12], and further developed in [13] and [14]. Essentially, it consists in computing the flow of a novel variable, defined as a particular function of the inverse propagator chosen in accordance to the structure of the original flow equations; so, for instance, the form of Eq. (23) suggests the introduction of the new variable $(h_k^{NSA})^{1/2-m}$ and the replacement of the flow equation of V_k with the one for this new variable.

Typically, the flow equation for this new variable, coupled with the one for Z_k , has a stabler behavior in proximity of the spinodal line. Then, it is convenient to take advantage of this alternative approach and therefore we checked the consistency of all our determinations, by comparing the output of the flow of the original variables and of the new ones.

Concerning the numerical methods adopted, we compared different approaches for each single determination of ΔE . Specifically, in one case we integrated the system of PDE by performing the spatial discretisation with a Chebyshev collocation method, and employing the method of lines to reduce the PDE to a system of ordinary differential equations. The resulting system is solved using a backward differentiation formula method, as encoded in the numerical libraries NAG [29].

As an alternative method, we have followed the approach of [12, 13] and we have used the MoL on a set of transformed equations for the threshold functions [14]. For actual calculations in this case we have employed the MoL as in Mathematica [30] with AccuracyGoal=10 and PrecisionGoal=10.

The first attempt to determine ΔE from the RG flow was obtained by solving the Wegner-Houghton equation [8–10]

$$\partial_t V_k = \frac{k}{2\pi} \log \left(1 + \frac{V_k(\varphi)''}{k^2} \right). \quad (30)$$

It is a single equation for the running potential V_k , and its generalization to include a renormalization factor Z_k is usually not taken into account as it contains some ambiguities [31, 32].

Then, by integrating Eq. (30), one finds a convex potential at $k = 0$, which is already a remarkable feature, because it is an exact property, [33], that can be recovered only within non-perturbative approaches (see, e.g., [34–36]) and, in addition, the gap is directly read from the value of the second derivative of the potential at the origin $\Delta E_{WH} = \sqrt{V_{k=0}(\varphi)''}|_{\varphi=0}$.

As a first exercise, we integrate Eq. (30) and the output is reported in the last column of Table I. As a consequence of the functional form of Eq. (30), the results are not extremely accurate and ΔE_{WH} in Table I are typically affected by an error of one or two units on the last displayed digit. We notice that when $M^2 = 1$, ΔE_{WH} differs from ΔE_{exact} of about 0.3% for $\lambda = 1$ and 0.1% for $\lambda = 0.02$ which shows the high accuracy of these findings in both regimes. The trend of ΔE_{WH} when $M^2 = -1$, will be discussed in Sect. III B, in comparison with other estimates.

B. Local Potential Approximation

$M^2 = 1$							
λ	ΔE_{exact}	ΔE_{erg}	ΔE_{pt1}	ΔE_{pt2}	ΔE_{pt3}	ΔE_{pt4}	ΔE_{pt10}
1	1.9341	1.9391	1.9361	1.9409	1.9428	1.9438	1.9458
0.02	1.0540	1.0542	1.0541	1.0542	1.0543	1.0543	1.0544
$M^2 = -1$							
λ	ΔE_{exact}	ΔE_{erg}	ΔE_{pt1}	ΔE_{pt2}	ΔE_{pt3}	ΔE_{pt4}	ΔE_{pt10}
0.4	0.9667	0.9785	0.9743	0.9810	0.9837	0.9852	0.9879
0.3	0.8166	0.8295	0.8254	0.8319	0.8345	0.8359	0.8386
0.2	0.6159	0.6314	0.6277	0.6336	0.6360	0.6373	0.6399
0.1	0.2969	0.3243	0.3241	0.3248	0.3256	0.3261	0.3272
0.05	0.0562	0.1120	0.1252	0.1049	0.0973	0.0932	0.0856
0.04	0.0210	0.0796	0.0939	0.0717	0.0635	0.0595	0.0532
0.03	0.0036	0.0545	0.0668	0.0481	0.0422	0.0395	0.0353
0.02	$0.93 \cdot 10^{-4}$	0.0341	0.0427	0.0299	0.0262	0.0246	0.0219
0.01	$1.05 \cdot 10^{-9}$	0.0161	0.0206	0.0141	0.0124	0.0116	0.0104

TABLE II: ΔE for various couplings λ and for $M^2 = 1$ or $M^2 = -1$, as obtained from the Schroedinger equation (ΔE_{exact}), the LPA ERG flow (ΔE_{erg}) and from the LPA PT flow with parameter $m = 1, 2, 3, 4, 10$ ($\Delta E_{pt1-pt10}$).

In Table II we report the numerical results obtained in the LPA, i.e. by keeping the renormalization fixed to $Z_k = 1$ along the flow, in the various cases corresponding to the ERG flow in Eqs. (9), (21) and to the PT flow in Eq. (24) for $m = 1, 2, 3, 4, 10$. With no correction due to the normalization factor Z_k , the gap in these computations is obtained as

$$\Delta E = \sqrt{V_{k=0}(\varphi)''}|_{\varphi=0} . \quad (31)$$

To facilitate the comparison, ΔE_{exact} , already shown in Table I, is again reported in Table II. We notice that, as expected, ΔE_{erg} always sits between the corresponding ΔE_{pt1} and ΔE_{pt2} .

Then, the content of Tables I and II is plotted in Fig. 1, and the points corresponding to various columns of these Tables are plotted with different colours and symbols, according to the legend

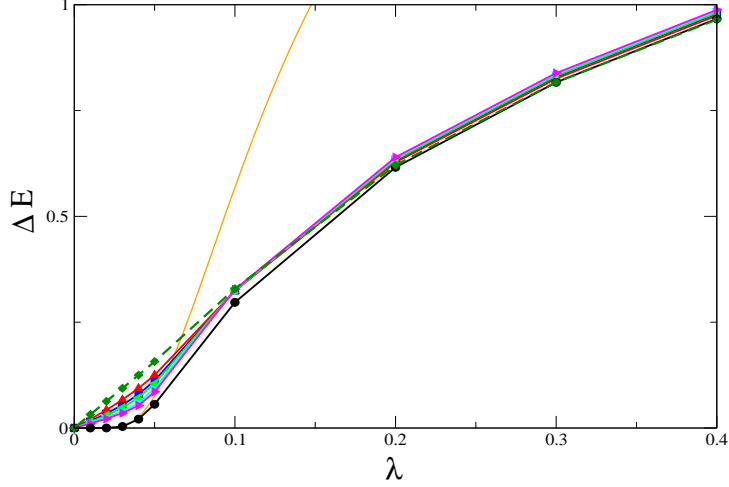


FIG. 1: Data reported in Tables I, II for ΔE as obtained in LPA, plotted as a function of the coupling λ . Lines joining the single points are included for convenience. ΔE_{exact} and ΔE_{WH} from Table I are respectively displayed as black circles with a continuous black line and green diamonds with a dashed green line. Then data from Table II are : blue squares, ΔE_{erg} ; red pointing up triangles, ΔE_{pt1} ; light green pointing left triangles, ΔE_{pt2} ; turquoise pointing down triangles, ΔE_{pt4} ; pink pointing right triangles, ΔE_{pt10} , all joined by continuous lines of the respective colour. The continuous orange line joins the instanton data of Table I.

reported in the Figure caption (note that, to avoid a redundant superposition of curves, in all figures we omit the data corresponding to ΔE_{pt3}). Fig. 2 shows three details of Fig. 1 for $\lambda = 0.4$, $\lambda = 0.2$ and $\lambda = 0.1$, while Fig. 3 is the enlargement of Fig. 1 in the region of smaller λ .

From Fig. 1 it is evident that all computations in the LPA produce accurate results only above $\lambda = 0.1$. In fact from the data in Table II we see that for $\lambda \geq 0.2$ the maximum distance of the various determinations from ΔE_{exact} is below 4% but it reaches 10% at $\lambda = 0.1$.

In Fig. 2 it is shown that at $\lambda = 0.4$ and $\lambda = 0.2$, ΔE_{WH} is the closest estimate to ΔE_{exact} , while at $\lambda = 0.1$ it becomes the farthest. At the same time, the distance from ΔE_{exact} of the PT estimates at various m grows with m , when $\lambda \geq 0.1$.

A totally different picture appears in Fig. 3 for $\lambda \leq 0.05$. In fact we observe that ΔE_{WH} approaches zero linearly with λ , then totally missing the exponential behavior of ΔE_{exact} . On the other hand, the LPA PT determinations invert their order and in this region the determinations with larger m show better agreement with ΔE_{exact} . In addition they also show a slight change of concavity that improves for larger m .

In summary, while our findings show that the LPA calculations are altogether satisfactorily accurate for $\lambda \geq 0.1$, on the contrary they are quantitatively inadequate to reproduce ΔE_{exact} when $\lambda \leq 0.05$. In this case, some improvement is necessary.

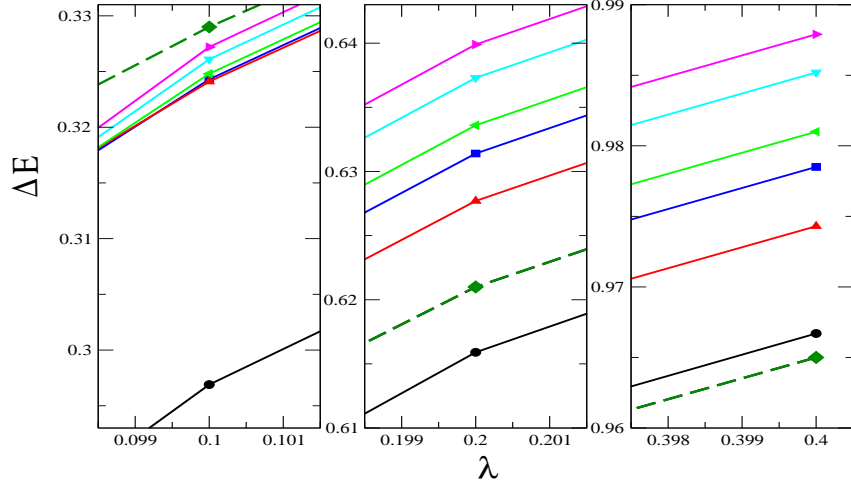


FIG. 2: Details of Fig.1 at three values of the coupling, $\lambda = 0.1, 0.2$ and 0.4 . Coding is given in Fig.1.

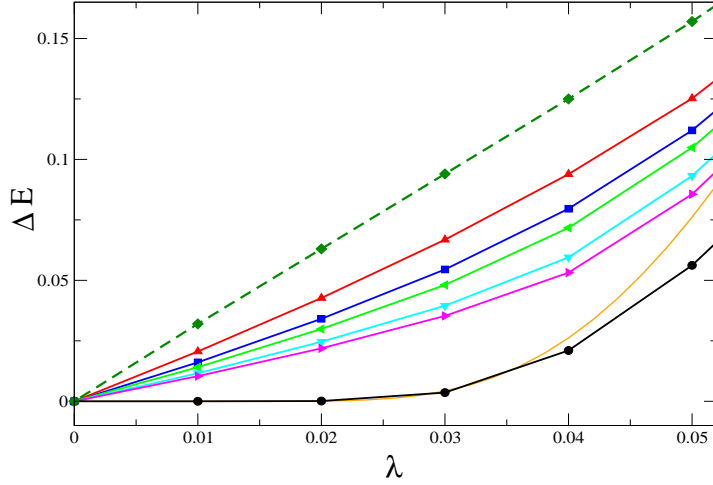


FIG. 3: Details of Fig.1 at small values of the coupling λ . Coding is given in Fig.1.

C. Inclusion of the renormalization Z_k

In this section we finally present the gap ΔE , corrected by the renormalization factor Z_k , i.e.

$$\Delta E = \sqrt{\frac{V_{k=0}(\varphi)''}{Z_{k=0}(\varphi)}} \Big|_{\varphi=0} \quad (32)$$

as obtained from the coupled flow equations for V_k and Z_k . Table III contains the results of the NSA ERG flow and of the NSA PT flow for $m = 1, 2, 3, 4, 10$, together with the corresponding value

of the correction $Z_{k=0}(\varphi = 0)$ displayed in parenthesis below. Again, the column with ΔE_{exact} is inserted for comparison.

$M^2 = 1$							
λ	ΔE_{exact}	ΔE_{erg}	ΔE_{pt1}	ΔE_{pt2}	ΔE_{pt3}	ΔE_{pt4}	ΔE_{pt10}
1	1.9341	1.9351 (1.0073)	1.9344 (1.010)	1.9365 (1.007)	1.9384 (1.007)	1.9395 (1.007)	1.9417 (1.006)
0.02	1.0540	1.5043 (0.9993)	1.0542 (1.0003)	1.0542 (1.0003)	1.0543 (1.0002)	1.0543 (1.0002)	1.0543 (1.0002)
$M^2 = -1$							
λ	ΔE_{exact}	ΔE_{erg}	ΔE_{pt1}	ΔE_{pt2}	ΔE_{pt3}	ΔE_{pt4}	ΔE_{pt10}
0.4	0.9667	0.9764 (1.037)	0.9632 (1.043)	0.9688 (1.033)	0.9723 (1.029)	0.9743 (1.027)	0.9782 (1.023)
0.3	0.8166	0.8276 (1.047)	0.8120 (1.055)	0.8182 (1.042)	0.8219 (1.037)	0.8239 (1.034)	0.8280 (1.029)
0.2	0.6159	0.6300 (1.074)	0.6083 (1.088)	0.6162 (1.065)	0.6203 (1.056)	0.6227 (1.052)	0.6271 (1.044)
0.1	0.2969	0.3158 (1.264)	0.2702 (1.356)	0.2888 (1.225)	0.2950 (1.188)	0.2980 (1.170)	0.3037 (1.140)
0.05	0.0562	X	X	0.0168 (7.503)	0.0262 (4.318)	0.0293 (3.648)	0.0333 (2.852)

TABLE III: ΔE for various couplings λ and for $M^2 = 1$ or $M^2 = -1$, as obtained from the Schroedinger equation (ΔE_{exact}) and from the coupled flow equation for V_k and Z_k , respectively in the NSA ERG case (ΔE_{erg}), and the NSA PT case with $m = 1, 2, 3, 4, 10$ ($\Delta E_{pt1-pt10}$). The correction $Z_k(\varphi = 0)$ is reported in parenthesis.

The NSA PT determinations of ΔE when $M^2 = 1$ strongly improve the agreement obtained with the LPA calculation. In fact, from Table III we observe that at $\lambda = 1$ the error for the worse determination (ΔE_{pt10}) is about 0.4%, but decreases to 0.02% for ΔE_{pt1} ; at $\lambda = 0.02$ the error is always around 0.03%. In addition, for both values of λ , we find $\Delta E_{pt1} \leq \Delta E_{erg} \leq \Delta E_{pt3}$ as in the LPA case. In all determinations, the correction factor $Z_{k=0}$ is extremely small.

By switching to the case $M^2 = -1$, for the PT case we find $\Delta E_{pt1} < \Delta E_{exact} < \Delta E_{pt10}$ for $\lambda > 0.1$, with an interval $(\Delta E_{pt10} - \Delta E_{pt1})/\Delta E_{pt10}$ of order 2% ÷ 3% if $\lambda > 0.2$, and around 10% at $\lambda = 0.1$. Instead, at $\lambda = 0.05$, we observe a rather different picture, because in the $m = 1$ case an imaginary component of the potential is generated and no clear convergence is observed whereas, at larger m , a definite value of ΔE together with very large $Z_{k=0} \gg 1$ is obtained but these estimates substantially differ from ΔE_{exact} .

For the NSA ERG data, we observe an unusual picture: in fact ΔE_{erg} is no longer similar to ΔE_{pt1} but it is rather closer to ΔE_{pt10} and, below $\lambda = 0.3$, it becomes even bigger: $\Delta E_{erg} > \Delta E_{pt10}$. At $\lambda = 0.05$, we do not find convergence to a definite value for ΔE_{erg} , much in the same way as it is observed for ΔE_{pt1} .

Finally, at smaller λ , no convergence is found, neither for the NSA PT case at any m , nor for the NSA ERG and we conclude that if $M^2 = 1$ the NSA determinations of the gap improve the LPA results, but if $M^2 = -1$, this is true only in the perturbative region ($\lambda > 0.1$ and $Z_{k=0} \sim 1$).

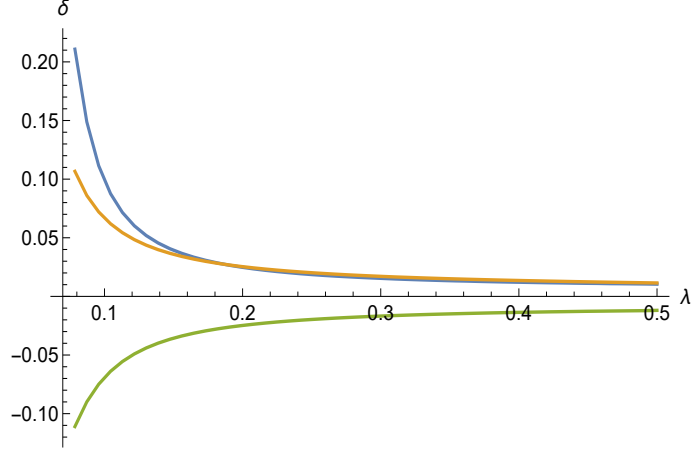


FIG. 4: Relative error $\delta = (\Delta E_{erg} - \Delta E_{exact})/\Delta E_{exact}$ for the SA ERG (blue upper positive curve), and for the simplified SA ERG with $\eta_k = 0$ (orange lower positive curve), and for the NSA ERG (green negative curve), vs. the coupling λ .

At smaller λ when the non-perturbative tunnelling effects become relevant, computations become impracticable.

Now we turn to the SA flow and show the output obtained in the ERG case, i.e. from the flow equations (21), (22), that include non-linear effects in the 'time' derivatives, due to the presence of η_k . Unfortunately, these non-linear terms substantially affect the numerical convergence of the PDE, and we can trust the results of this scheme only for $\lambda \geq 0.08$. In order to get some insight, we report in Fig. 4 the relative error on the determinations $\delta = (\Delta E_{erg} - \Delta E_{exact})/\Delta E_{exact}$ as a function of the coupling $\lambda \geq 0.08$, for the SA ERG (blue upper positive curve).

The determination of δ for the NSA ERG (green negative curve) is also included for comparison. We observe that the relative error becomes larger for smaller values of the coupling in both cases, but δ of the SA ERG is about twice the one of the NSA ERG at $\lambda = 0.08$. We also performed the analysis of the SA PT flow corresponding to the 'B-scheme' of [27] but we do not report the corresponding curve, as it essentially produces even worse results than those of the SA ERG scheme, shown by the blue curve in Fig. 4.

Instead, the computation of the simplified SA ERG flow, where the nonlinear effects in Eqs. (21) and (22) are discarded by taking $\eta_k = 0$, turns out to be much stabler than the full SA (ERG and PT) flows. This is evident from the plot of the corresponding δ (red lower positive curve) in Fig. 4, which is of the same size (although opposite in sign) of the NSA ERG relative error.

On the PT side, the flow that can consistently be compared with the SA ERG flow with $\eta_k = 0$, corresponds to the 'simplified type-C scheme' of [27], reported in Eqs. (27), (28). In fact, we integrated these two SA simplified flows and, in addition to a small relative error, we also found in both cases convergence at smaller values of the coupling, so that our analysis could be pushed down to $\lambda = 0.03$. Therefore, below, we discuss in more detail the output of these two sets of PDE, namely Eqs. (21), (22) and (27), (28), as representative respectively of the ERG SA and PT SA flow, and the relative data are reported in Table IV and also collectively shown in Fig.5.

A comparison of Fig.5 and Fig.1 clearly indicates that the agreement of the SA data with ΔE_{exact} is improved with respect to the LPA data in the region of small λ . In addition, from Table IV we find $\Delta E_{pt1} < \Delta E_{erg} < \Delta E_{pt2}$, with the exception of the smallest values of the coupling $\lambda = 0.04$ and $\lambda = 0.03$, which we shall comment on later. In both rows with $M^2 = 1$ in Table IV, we find $\Delta E_{pt1} < \Delta E_{exact} < \Delta E_{pt10}$, but it must be remarked that the difference $\Delta E_{pt10} - \Delta E_{pt1}$,

$M^2 = 1$							
λ	ΔE_{exact}	ΔE_{erg}	ΔE_{pt1}	ΔE_{pt2}	ΔE_{pt3}	ΔE_{pt4}	ΔE_{pt10}
1	1.9341	1.9249 (1.009)	1.9197 (1.010)	1.9279 (1.008)	1.9311 (1.007)	1.9329 (1.007)	1.9362 (1.006)
0.02	1.0540	1.0539 (1.003)	1.0538 (1.0003)	1.0540 (1.0003)	1.0541 (1.0002)	1.0543 (1.0002)	1.0542 (1.0002)
$M^2 = -1$							
λ	ΔE_{exact}	ΔE_{erg}	ΔE_{pt1}	ΔE_{pt2}	ΔE_{pt3}	ΔE_{pt4}	ΔE_{pt10}
0.4	0.9667	0.9514 (1.040)	0.9427 (1.048)	0.9564 (1.035)	0.9617 (1.031)	0.9645 (1.029)	0.9699 (1.024)
0.3	0.8166	0.8011 (1.051)	0.7922 (1.062)	0.8062 (1.045)	0.8116 (1.039)	0.8144 (1.036)	0.8200 (1.031)
0.2	0.6159	0.5994 (1.082)	0.5899 (1.101)	0.6049 (1.071)	0.6105 (1.061)	0.6136 (1.056)	0.6192 (1.047)
0.1	0.2969	0.2769 (1.308)	0.2660 (1.400)	0.2844 (1.245)	0.2905 (1.204)	0.2935 (1.185)	0.2994 (1.151)
0.05	0.0562	0.0334 (5.872)	0.0306 (7.328)	0.0483 (3.291)	0.0516 (2.763)	0.0527 (2.559)	0.0539 (2.255)
0.04	0.0210	0.0013 (138.2)	0.0027 (80.51)	0.0141 (8.649)	0.0167 (6.252)	0.0178 (5.397)	0.0224 (3.162)
0.03	0.0036	X	0.0016 (90.71)	0.0015 (14.67)	0.0036 (11.27)	0.0059 (6.51)	0.0099 (3.85)

TABLE IV: Same as in Table III, but with ΔE derived from the SA ERG flow in Eqs. (21), (22) and SA PT flow in Eqs. (27), (28).

although smaller than 1% in the two cases, is twice the corresponding difference for the NSA case.

Turning to the $M^2 = -1$ problem, a picture of the data obtained at $\lambda = 0.4, 0.2, 0.1$ is given in the three panels of Fig.6 where, together with ΔE_{exact} (black circles), the SA determination of ΔE_{pt1} (red triangles pointing up) and of ΔE_{pt10} (pink triangles pointing right) and, in addition, also the NSA determination of ΔE_{pt1} (red stars) and of ΔE_{pt10} (pink crosses) are displayed. In all panels the point ΔE_{exact} is always between the ΔE_{pt10} and ΔE_{pt1} and the distance between these two determinations is smaller for the NSA case at $\lambda = 0.4$ but it becomes practically equal to the one for the SA case at $\lambda = 0.1$. At smaller coupling λ , as already seen, the NSA flow fails to converge and only the SA determinations are available at very low λ .

Finally, the region of $\lambda \leq 0.05$ is displayed in Fig.7 where the SA determinations are plotted together with ΔE_{exact} and ΔE_{inst} . Fig.7 clearly shows the importance of the inclusion of $Z_{k=0}$ (which has now values of order 10 or in some cases even 100) : points that in the LPA approximation are very far from ΔE_{exact} , now have substantially reduced their distance.

In particular, even the worst determination (ΔE_{pt1}) at $\lambda = 0.05$ shows an agreement (about 35%) very similar to that of the instanton calculation. At $\lambda = 0.04$, while ΔE_{pt1} and ΔE_{erg} become very small, calculations at larger m (e.g. $m = 10$) are reasonably accurate, with error below 10%.

At $\lambda = 0.03$, ΔE_{inst} still differs from ΔE_{exact} of about 30%, while the PT determinations at $m = 1$ and $m = 2$ are off of 45%. The case with $m = 3$ (not reported in Fig.7 - see Table IV)

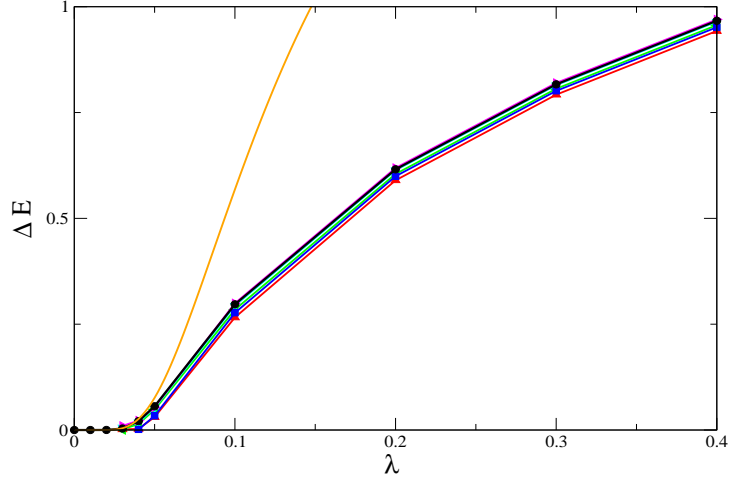


FIG. 5: Data reported in Table IV for ΔE , as obtained by including the correction Z_k in the simplified SA scheme, plotted vs. λ . Again, for convenience, lines joining the points are included. Also the same coding as in Fig. 1 is adopted, with the exception of ΔE_{WH} data, not included here as no Z_k correction is available.

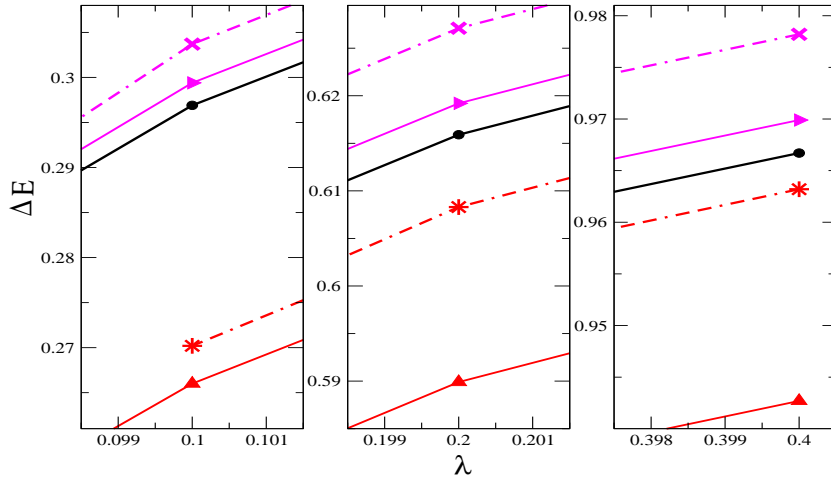


FIG. 6: Details of ΔE , including the correction Z_k , at three values of the coupling $\lambda = 0.1, 0.2, 0.4$. In addition to ΔE_{exact} data from Table I (black circles with a continuous black line), we plot ΔE_{pt1} and ΔE_{pt10} from Table III for the NSA case, respectively with red stars and pink crosses, both with dot-dashed lines of the respective colour attached. Moreover, ΔE_{pt1} and ΔE_{pt10} from Table IV for the SA case, are plotted with the same coding as in Figs.1 and 5, i.e. the former with red triangles pointing up and the latter with pink triangles pointing right. Both have continuous lines of the respective colour attached.

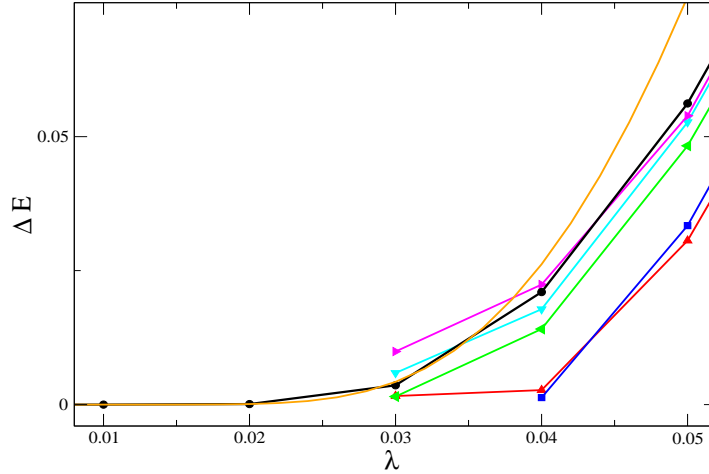


FIG. 7: Details at small values of λ of Fig.5. ΔE , including the correction Z_k , is plotted vs. λ . Coding is the same as in Figs.1, 5 and 6.

practically reproduces ΔE_{exact} , and $m = 10$ yields too large values of the gap. Instead, the ERG flow fails to converge at $\lambda = 0.03$, and this is probably due to an increasing Z_k as $k \rightarrow 0$ (already at $\lambda = 0.04$ we find $Z_{k=0} = 138$) that reduces the gap to such a small value to be comparable with the numerical precision.

The same kind of problem is observed at $\lambda = 0.02$ not only for the ERG flow, but also for the PT flow with $m = 1$ and $m = 2$. Yet, at $m = 3, 4, 10$ we find convergence, respectively to $3 \cdot 10^{-4}$, $9 \cdot 10^{-4}$, $3.4 \cdot 10^{-3}$ which, at least for $m = 3$, is of the same order of magnitude of ΔE_{exact} ; however we prefer not to report these values in Table IV because, especially for the first two cases, they are comparable with the numerical precision of our computation.

Therefore, we conclude that, when including the correction $Z_{k=0}$, our computation qualitatively reproduces the exponential trend induced by the tunnelling in the region $\lambda = 0.03 - 0.05$.

IV. CONCLUSIONS

The computation of the energy gap in the quanta-mechanical double well potential by means of the derivative expansion of the Functional Renormalization Group flow equations performed in this paper, essentially aims at understanding to which extent this approach can quantitatively keep under control the simplest one-dimensional non-perturbative effect, associated to the tunneling between the two vacua. Therefore, we mainly focus on the comparison of the average estimates of various formulations of the flow equations with the accurate results coming from the Schrodinger equation resolution of the problem.

The improvement associated to the inclusion of higher terms of the derivative expansion is evident even in the case of the anharmonic oscillator with $M^2 = 1$, as shown in Tables II, III, IV. In this case, the agreement of our estimates is always excellent (with a relative error that never exceeds 1%), but the improvement when going from the LPA in Table II to the the NSA approximation in Table III and simplified SA in Table IV, is evident especially in the large coupling

case $\lambda = 1$.

Turning to the double well case with $M^2 = -1$, we can clearly distinguish different regimes associated to the explored range λ . Fig. 1 shows that the estimates obtained in LPA for $\lambda \geq 0.2$ are globally accurate; then, for lower λ the agreement diminishes and for $\lambda \geq 0.05$, this approximation hardly reproduces the exponential approach to zero of ΔE . As shown in Fig. 3, the WH approach has an inaccurate linear behavior, while for instance the PT potential with $m = 10$ shows a qualitative agreement with the exact values.

Then, the inclusion of Z_k in the simplified SA version of the flow equations, clearly brings a strong improvement in the region $0.1 \leq \lambda \leq 0.03$ as seen in Figs. 5 and 7. Even at $\lambda = 0.04$, some estimates turn out to be more accurate than the instanton determination of ΔE , which is then no longer valid at $\lambda = 0.03$ where ΔE_{inst} becomes the most precise estimate displayed. However, it must be remarked that already at $\lambda = 0.04$, and more evidently at smaller λ , not all formulations of the flow equations show clear convergence within our numerical precision. This drawback becomes too strong at $\lambda = 0.02$ and we do not trust our findings at this value of the coupling.

To summarize, the inclusion of the first correction to the LPA represents a strong improvement in the range $0.1 \leq \lambda \leq 0.03$, indicating that the derivative expansion of the RG flow does actually reproduce the non-perturbative exponential decay of ΔE . It is conceivable to expect that the next step in the derivative expansion, corresponding to inclusion of four derivatives in the original action, could further enhance the convergence of the PDE for $\lambda \leq 0.03$.

A final comment is dedicated to the different approaches adopted in our analysis. We found that, both NSA and SA (in either full or simplified version) are equally accurate as long as the wave function renormalization $Z_k \sim 1$, as shown in Fig. 4. But, as soon as Z_k grows up to non-perturbative values, the NSA and the full SA schemes become not trustable or do not converge, the former because of the incomplete cancellation of the term $Z_k p^2$ in the propagators, and the latter because of the presence of non-linear terms in the 'time' derivative of Z_k , included in η_k . In both cases the growth of Z_k has these undesired effects. Still, in the simplified SA approach, where these problems are circumvented, PDE are integrated at much lower values of λ and, at least in the PT flow with m suitably optimized, providing precise estimates of ΔE .

Acknowledgments

This work has been partially supported by the INFN project FLAG. AB would like to thank Manuel Reichert for comments on the manuscript.

-
- [1] N. Dupuis, L. Canet, A. Eichhorn, W. Metzner, J. Pawłowski, M. Tissier, and N. Wschebor, *Physics Reports* **910**, 1 (2021), ISSN 0370-1573, the nonperturbative functional renormalization group and its applications, URL <https://www.sciencedirect.com/science/article/pii/S0370157321000156>.
 - [2] S. Coleman, *Aspects of Symmetry: Selected Erice Lectures* (Cambridge University Press, Cambridge, U.K., 1985), ISBN 978-0-521-31827-3.
 - [3] J. Zinn-Justin, *Quantum Field Theory and Critical Phenomena; 4th ed.*, International series of monographs on physics (Clarendon Press, Oxford, 2002), URL <https://cds.cern.ch/record/572813>.
 - [4] F. Devoto, S. Devoto, L. Di Luzio, and G. Ridolfi (2022), 2205.03140.
 - [5] F. L. Bezrukov and M. Shaposhnikov, *Phys. Lett. B* **659**, 703 (2008), 0710.3755.

- [6] E. Bentivegna, V. Branchina, F. Contino, and D. Zappalà, *JHEP* **12**, 100 (2017), 1708.01138.
- [7] V. Branchina, E. Bentivegna, F. Contino, and D. Zappalà, *Phys. Rev. D* **99**, 096029 (2019), 1905.02975.
- [8] A. Horikoshi, K.-I. Aoki, M.-a. Taniguchi, and H. Terao, in *Workshop on the Exact Renormalization Group* (1998), pp. 194–203, hep-th/9812050.
- [9] K. I. Aoki, A. Horikoshi, M. Taniguchi, and H. Terao, *Prog. Theor. Phys.* **108**, 571 (2002), quant-ph/0208173.
- [10] A. S. Kapoyannis and N. Tetradis, *Phys. Lett. A* **276**, 225 (2000), hep-th/0010180.
- [11] D. Zappala, *Phys. Lett. A* **290**, 35 (2001), quant-ph/0108019.
- [12] A. Parola, D. Pini, and L. Reatto, *Phys. Rev. E* **48**, 3321 (1993), URL <https://link.aps.org/doi/10.1103/PhysRevE.48.3321>.
- [13] A. Bonanno and G. Lacagnina, *Nucl. Phys. B* **693**, 36 (2004), hep-th/0403176.
- [14] J.-M. Caillol, *Nucl. Phys. B* **855**, 854 (2012), 1109.4024.
- [15] W. Ames, W. Rheinboldt, and A. Jeffrey, *Numerical Methods for Partial Differential Equations*, Applications of mathematics series (Academic Press, 1977), ISBN 9780177710865, URL <https://books.google.it/books?id=MCrvAAAAAAAJ>.
- [16] M. Weyrauch, *J. Phys. A* **39**, 649 (2006).
- [17] F. Synatschke, G. Bergner, H. Gies, and A. Wipf, *JHEP* **03**, 028 (2009), 0809.4396.
- [18] J. Kovacs, S. Nagy, and K. Sailer, *Int. J. Mod. Phys. A* **30**, 1550058 (2015), 1403.3544.
- [19] H. Gies, *Phys. Rev. D* **66**, 025006 (2002), hep-th/0202207.
- [20] C. Wetterich, *Phys. Lett. B* **301**, 90 (1993), 1710.05815.
- [21] T. R. Morris, *Int. J. Mod. Phys. A* **9**, 2411 (1994), hep-ph/9308265.
- [22] D. F. Litim and J. M. Pawłowski, *Phys. Lett. B* **546**, 279 (2002), hep-th/0208216.
- [23] D. F. Litim, *Phys. Lett. B* **486**, 92 (2000), hep-th/0005245.
- [24] A. Bonanno and D. Zappala, *Phys. Lett. B* **504**, 181 (2001), hep-th/0010095.
- [25] A. Bonanno and M. Reuter, *JHEP* **02**, 035 (2005), hep-th/0410191.
- [26] S. P. de Alwis, *JHEP* **03**, 118 (2018), 1707.09298.
- [27] A. Bonanno, S. Lippoldt, R. Percacci, and G. P. Vacca, *Eur. Phys. J. C* **80**, 249 (2020), 1912.08135.
- [28] D. F. Litim and J. M. Pawłowski, *Phys. Lett. B* **546**, 279 (2002), hep-th/0208216.
- [29] NAG, *The Numerical Algorithms Group*, Oxford, United Kingdom, URL www.nag.com.
- [30] W. R. Inc., *Mathematica, Version 12.1* (2020), champaign, IL, 2020, URL <https://www.wolfram.com/mathematica>.
- [31] A. Bonanno and D. Zappala, *Phys. Rev. D* **57**, 7383 (1998), hep-th/9712038.
- [32] A. Bonanno, V. Branchina, H. Mohrbach, and D. Zappala, *Phys. Rev. D* **60**, 065009 (1999), hep-th/9903173.
- [33] K. Symanzik, *Commun. Math. Phys.* **16**, 48 (1970).
- [34] D. J. E. Callaway and D. J. Maloof, *Phys. Rev. D* **27**, 406 (1983).
- [35] D. J. E. Callaway, *Phys. Rev. D* **27**, 2974 (1983).
- [36] V. Branchina, P. Castorina, and D. Zappala, *Phys. Rev. D* **41**, 1948 (1990).